Physics Letters B 762 (2016) 263–270

Contents lists available at ScienceDirect

Physics Letters B

www.elsevier.com/locate/physletb

Transition from direct to sequential two-proton decay in *s–d* shell nuclei

T.A. Golubkova [a], X.-D. Xu [b,c,d], L.V. Grigorenko [e,f,g,*], I.G. Mukha [c,g], C. Scheidenberger [b,c], M.V. Zhukov [h]

[a] *Advanced Educational and Scientific Center, Moscow State University, Kremenchugskaya 11, 121357 Moscow, Russia*
[b] *II. Physikalisches Institut, Justus-Liebig University, 35392 Giessen, Germany*
[c] *GSI Helmholtzzentrum für Schwerionenforschung, 64291 Darmstadt, Germany*
[d] *School of Physics and Nuclear Energy Engineering, Beihang University, 100191 Beijing, China*
[e] *Flerov Laboratory of Nuclear Reactions, JINR, 141980 Dubna, Russia*
[f] *National Research Nuclear University "MEPhI", Kashirskoye shosse 31, 115409 Moscow, Russia*
[g] *National Research Centre "Kurchatov Institute", Kurchatov sq. 1, 123182 Moscow, Russia*
[h] *Department of Physics, Chalmers University of Technology, S-41296 Göteborg, Sweden*

ARTICLE INFO

Article history:
Received 3 May 2016
Received in revised form 1 September 2016
Accepted 4 September 2016
Available online 21 September 2016
Editor: D.F. Geesaman

Keywords:
Dripline *s–d* shell nuclei
One-proton, two-proton decay
Two-proton emission mechanisms
Transitions between different modes of two-proton emission
Two-proton decays of ^{15}Ne and ^{30}Ar

ABSTRACT

The transition between different mechanisms of two-proton decay in exotic nuclei and the governing physical conditions are generally studied. To perform this large-scale survey, the direct-decay model, which is widely used, was improved by generalizing the semi-analytical approaches used before. The improved model provides a flawless phenomenological description of three-body correlations in $2p$ decays, as is demonstrated by several examples of decays of low-lying states in ^{16}Ne. Different transition mechanisms are shown to occur beyond the proton dripline for *s–d* shell nuclei. It is found that the transition dynamics of $2p$-emitters allows the extraction of the width of the ground-state resonance of the core $+ p$ subsystem. The practical application of the method is illustrated by determining properties of the ^{14}F ground state derived from the $^{15}\mathrm{Ne} \rightarrow {}^{13}\mathrm{O} + 2p$ decay data, and of the ^{29}Cl ground state derived from the $^{30}\mathrm{Ar} \rightarrow {}^{28}\mathrm{S} + 2p$ decay data.

© 2016 The Author(s). Published by Elsevier B.V. This is an open access article under the CC BY license (http://creativecommons.org/licenses/by/4.0/). Funded by SCOAP[3].

1. Introduction

Two-proton ($2p$) radioactivity has attracted a large interest in theory and experiment in recent years. This peculiar radioactive decay mode was predicted for even-proton systems in the year 1960 [1] and experimentally discovered in 2002 [2,3]. Since then, important advances in the studies of two-proton ($2p$) radioactivity, and, more generally speaking, of *true two-proton decays* [4] were made. These studies comprise part of a general effort to extend our knowledge to the limits of existence of nuclei, up to the neutron and proton driplines and as far beyond them as possible. It is known that the true $2p$ decay mechanism, where both protons are emitted *simultaneously*, is realized under certain energetic conditions, in particular when the relation between one- and two-proton separation energies (S_p and S_{2p}, respectively) makes *sequential decay* (two single-proton emissions separated in time) impossible: $S_{2p}^{(A)} < 0$ and $S_p^{(A)} > 0$, where A denotes the mass number of the mother nucleus. However, in light proton-rich and in neutron-rich nuclei, where the potential barriers governing the decay are relatively small, the genuine three-body decay mechanism can materialize in the form of a *democratic decay* [5]: these democratic decays exhibit distinct correlations between the decay products and follow a different systematic of lifetimes compared to *true* $2p$ decays [4]. Together, and at variance to the *sequential* decay mechanism, which requires the population of intermediate narrow states, the true $2p$ and democratic decays are often characterized as *direct* decays. A schematic view of the various decay mechanisms and their energy balance is shown in Fig. 1 (a,b,d,e).

The transition from the true $2p$ mechanism to the democratic decay dynamic is typically governed by the relation of the two quantities, Γ_r (the width of the resonance ground state) and E_r (the ground state decay energy in the core $+ p$ subsystem of the three-body system core $+ p + p$). The characteristic of this transition and the underlying physics have so far not been considered

* Corresponding author.
E-mail address: lgrigorenko@yandex.ru (L.V. Grigorenko).

http://dx.doi.org/10.1016/j.physletb.2016.09.034
0370-2693/© 2016 The Author(s). Published by Elsevier B.V. This is an open access article under the CC BY license (http://creativecommons.org/licenses/by/4.0/). Funded by SCOAP[3].

systematically. This is the purpose of the present Letter, and the motivation will be further detailed in the following.

In general, the decay dynamics of $2p$ emission is fully characterized by three parameters: (i) the $2p$ decay energy $E_T = -S_{2p}^{(A)}$, (ii) the ground state (g.s.) decay energy in the core $+\ p$ subsystem $E_r = -S_p^{(A-1)} = S_p^{(A)} - S_{2p}^{(A)}$, and (iii) the width Γ_r of the intermediate state. As the width Γ_r is a function of E_r, the delimitation of different $2p$ decay mechanisms can be depicted by a kind of "phase diagram" in the $\{E_T, E_r\}$ plane, see Fig. 1 (c).

The transitions between different mechanisms (or decay dynamics) were rudimentary mentioned in previous works [4,6–8]. Here, Fig. 1 provides an overall view of the transition dynamic in $2p$ decays. At first glance, one would expect that the direct $2p$ and the sequential decay are separated by the line where $E_r = E_T$. However, it was shown in Refs. [6,7] that this transition happens at lower values $E_r = (0.75\text{–}0.85)E_T$. Similarly, it was found experimentally for decays of ^{6}Be and ^{16}Ne in Refs. [9,10] that the transition "Democratic $2p$"↔"Sequential $2p$" does not even happen for energies E_T considerably higher than $E_T = 2E_r$; this issue remains an open question. In the present work we investigate systematically the transition regime "True $2p$"↔"Sequential $2p$", and, while moving along this line, we obtain detailed quantitative results for the transition region "True $2p$"↔"Democratic $2p$" in Section 5. It is demonstrated that this transition region is often involved in ground-state decays of s–d shell nuclei beyond the proton dripline.

Besides the general interest, there is another motivation for the present study, which has practical impact. Any phenomena of the transition type are expected to be prone to abrupt changes of its properties in response to minor variation of the parameters. Here even small variations of the characteristic decay parameters can lead to strong modifications of the decay properties and observed quantities (such as branching ratios, lifetimes, etc.). In turn, this sensitivity can be used for a precise derivation of the nuclear parameters from measurements or for imposing limitations on their relations. Among the relevant parameters $\{E_T, E_r, \Gamma_r\}$, the most interesting one is the sensitivity to Γ_r. While resonance energies can be determined with rather good precision from available experimental data, much better resolution and/or statistics is required to derive the width of a state. The latter conditions are presently often not attainable for exotic dripline systems. Moreover, there is a rather large experimental "blind spot" with respect to the g.s. resonance widths, which covers the interval from ~ 1 meV to ~ 10 keV (corresponding to resonance lifetimes ranging from $\sim 10^{-19}$ s to ~ 1 ps): the invariant and missing mass methods using spectrometers or kinematical complete measurements can be applied when resonance widths exceed ~ 10 keV (i.e.: resonance lifetimes $\lesssim 10^{-19}$ s), while other techniques (such as the in-flight decay method, plunger, *etc.*) are applicable only for long-lived states with lifetimes exceeding a few picoseconds (i.e.: widths $\lesssim 1$ meV). Therefore, we derive here an indirect method to obtain information on the widths Γ_r of the proton subsystems in the transition regimes between different mechanisms of two-proton emission. The practical feasibility of this method is demonstrated with the examples of ^{14}F g.s. populated in the $2p$ decay of the ^{15}Ne g.s. [11] and of ^{29}Cl g.s. populated in the $2p$ decay of ^{30}Ar [12].

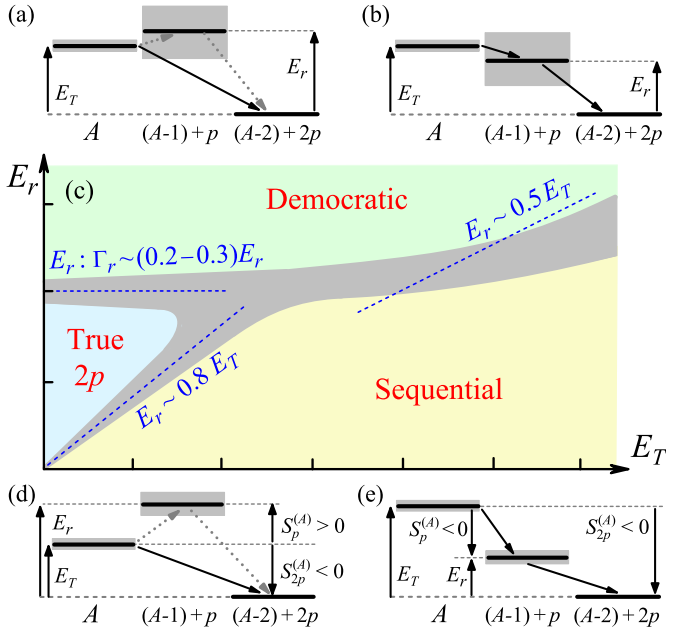

Fig. 1. (Color online.) Energy conditions for various possibilities of how $2p$-decays can materialize: (a) as democratic decay directly to the daughter nucleus or (b) via broad intermediate states, (d) as true $2p$-decay, also referred to as $2p$-radioactivity, or (e) as sequential decay via narrow intermediate states. The true and democratic decays are usually summarized as "direct decays". A schematic sketch of different $2p$ decay regimes in the $\{E_T, E_r\}$ plane is shown in panel (c): true, democratic, and sequential mechanisms are indicated by different colors. The transition region separating these regimes is shown in gray color. The dashed lines delineating the boarderline of the transition region correspond to the displayed ratios between the $2p$-decay energies E_T in a three-body system and the $1p$-decay energies E_r of the g.s. of the core $+\ p$ subsystem.

2. Dynamics of three-body systems near the proton dripline

As mentioned above, the relationship of $S_p^{(A)}$ and $S_{2p}^{(A)}$ is one of the decisive conditions for different forms of nuclear dynamics in the even-proton systems in the proximity of the proton dripline. To illustrate this behavior, the systematics of the p and $2p$ separation energies for Ne and Ar isotopes near the proton dripline is shown in Fig. 2. These nuclides represent the lower and the upper parts of the s–d shell, respectively. One can see that the evolution of $S_p^{(A)}$ and $S_{2p}^{(A)}$ values is different, and the corresponding curves intersect near the proton dripline, leading to rapid changes of the dynamical properties of nuclides in this region. Particle-stable nuclei that are closest to the dripline typically exhibit a so-called Borromean structure (this denotes the phenomenon that removal of one of the three bodies, either one of the two protons or the core, leads to disintegration of the whole three-body system) with the condition $S_p^{(A)} > S_{2p}^{(A)}$. Particle-unstable nuclei located just beyond the dripline often undergo direct decays, i.e. either $2p$ decay by the true ($S_{2p}^{(A)} < 0$, $S_p^{(A)} > 0.2S_{2p}^{(A)}$) or by the democratic ($S_{2p}^{(A)} < 0$, $S_p^{(A)} \sim 0$) mechanism; in addition, a transition situation is possi-

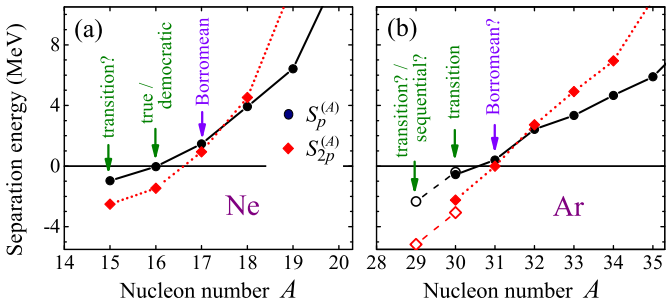

Fig. 2. (Color online.) Systematics of p and $2p$ separation energies ($S_p^{(A)}$ and $S_{2p}^{(A)}$, respectively) for neon [panel (a)] and argon [panel (b)] isotopes, which are shown by circles and diamonds, respectively. The hollow symbols in panel (b) joined by a dashed line show the mass predictions from Ref. [13]. Isotopes with specific structure and decay properties defined by the ratios of the $S_p^{(A)}$ and $S_{2p}^{(A)}$ values are highlighted by arrows and the corresponding text legends.

ble. Nuclei located further beyond the dripline pass the transition area and arrive either at a domain of democratic $2p$ decays (very likely for the lightest nuclei) or at a domain of sequential $2p$ decays (rather expected for the heavier, higher-Z systems). Thus, the transition dynamics investigated here is a quite likely situation in the area between the direct (true or democratic) and sequential $2p$-decay dominance.

3. Improved direct $2p$-decay model

Simplified analytical models of $2p$ decay are useful theoretical tools, which can substitute complicated and time-consuming three-body calculations when "quick" estimates, systematic studies, or just a phenomenological comparison with experimental observations is needed. The derivation of the direct decay model for $2p$ emission was described in detail in Refs. [7,14]. The model is based on the utilization of simplified three-body Hamiltonians, which allow a factorization of the Green's function. This approach can be traced back to the ideas of Galitsky and Cheltsov [15]. The expressions originating from the resonant R-matrix-type approximation [14] look very similar to those arising from the quasi-classical approximation [16], later used for $2p$ emission in a number of works [17,18, and references therein]. However, the models have important differences, which are discussed for example in [4, 14,19].

The direct decay models of Refs. [7,14] have some disadvantages, which are overcome in the present approach. Namely, the decay amplitudes must be factorized either in the "V" system [see Fig. 3 (a)], or in one of the "Y" systems [see Fig. 3 (b,c)]. In the "V" system, the anti-symmetrization between identical protons is straightforward. However, the assumption of an infinite core mass is required in this case. Also the interaction of the protons (including Coulomb repulsion) is neglected, which leads to some overestimation of the width. This type of approximation is called "no p–p Coulomb" (NPP), see Eq. (21) of Ref. [7]. Working in the "Y" systems, the p–p Coulomb interaction can be effectively considered by taking the $Z_i Z_j$ term of the Coulomb interaction in the X dimension as Z_c while in the Y coordinate as Z_c+1. Unfortunately, a consistent anti-symmetrization is complicated in the "Y" system, and one of the core + p resonances is not treated appropriately. That is because the X coordinate is exactly the vector between core and p, but the Y coordinate is only approximately equal to the vector between the core and another p. The latter approximation becomes exact in the limit $A_c \to \infty$ (in this limit "Y"→"V"). This approximation is called "effective p–p Coulomb" (EFC), see Eq. (22) of Ref. [7].

In the following, an improved direct decay model (IDDM) is developed which is based on simple R-matrix-type analytical approximations for amplitudes; it combines the positive features of both approximations, NPP and EFC. The general expression derived in Ref. [7] [see Eqs. (30)–(32) of this work], however with a modification, which accounts in a correct way for the angular momentum

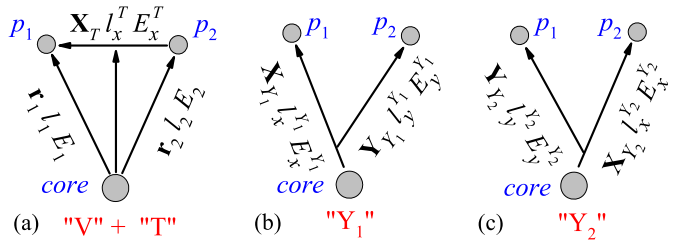

Fig. 3. (Color online.) Three coordinate systems, "V"+"T", "Y_1", "Y_2", with their respective kinematical variables as used in this work for the description of the three-body system core + p + p, are shown in panels (a), (b), and (c), respectively.

coupling of $\{j_1, l_1\}$ and $\{j_2, l_2\}$ of the first and the second core + p subsystems, is:

$$\frac{d\Gamma(E_{3r})}{d\Omega_\varkappa} = \frac{8E_{3r}}{\pi(2J+1)} \sum_{M_J} \left| \sum_\gamma A_\gamma^{JM_J}(\varepsilon, \Omega_1, \Omega_2) \right|^2 , \tag{1}$$

where J is the total angular momentum, $\gamma = \{j_1, l_1, j_2, l_2\}$, $\Omega_\varkappa = \{\varepsilon, \Omega_1, \Omega_2\}$, and the angles Ω_i are related to the vectors $\mathbf{r}_i$ (see Fig. 3). The amplitude $A_\gamma^{JM_J}$ is defined as

$$A_\gamma^{JM_J}(\Omega_\varkappa) = \frac{[j_1 \otimes j_2]_{JM_J}}{\sqrt{\nu_1 \nu_2}} \int_0^R dr_1' \int_0^R dr_2' \, \varphi_{j_1 l_1}(k_1 r_1') \times \varphi_{j_2 l_2}(k_2 r_2') \, \Delta V(r_1', r_2') \, \varphi_{J\gamma}(r_1', r_2') , \tag{2}$$

where $\varphi_{J\gamma}$ is assumed to be the radial part of the three-body resonant wave function (WF) in jj coupling. The nature of the short-range potential ΔV and its derivation and the underlying approximations are discussed in detail in Ref. [7]. The amplitude A^{JM_J} does not depend on the parameter R when it is chosen beyond the range of ΔV. The integral in Eq. (2) can be evaluated by replacing the continuum WFs with the quasi-stationary WF in proximity of the two-body resonance energies:

$$\varphi_{jl}(kr) = \frac{\sqrt{\nu(E)}}{2} A_{jl}(E) \, \hat{\psi}_{jl}(E_r, r) , \tag{3}$$

where k, ν, E are the related momentum, velocity, and energy in the two-body channel. The pure radial function $\hat{\psi}_{jl}(E_r, r)$ is the quasi-bound WF: it has a resonant boundary condition at the two-body resonant energy E_r and is normalized to unity in the internal domain as

$$\hat{\psi}_{jl}(E_r, r > R) \propto G_l(k_r r) , \quad \int_0^R dr \left| \hat{\psi}_{jl}(E_r, r) \right|^2 = 1 ,$$

where G_l is irregular at the origin Coulomb WF with angular momentum l. In this definition, the value of parameter R should be chosen around the classical outer turning points for the core + p Coulomb barriers. The amplitude A_{jl} of the resonance with the parameters E_r and $\Gamma_r = \Gamma(E_r)$ is defined as

$$A_{jl}(E) = \frac{\sqrt{\Gamma(E)}}{E_r - E - i\Gamma(E)/2} + A_{jl}^{(p)}(E) . \tag{4}$$

The width as a function of energy is defined by the standard R-matrix expression

$$\Gamma(E) = 2 \frac{\theta^2}{2Mr_{cp}^2} P_l(Z_1, Z_2, r_{cp}, E) , \tag{5}$$

via the penetrability function P_l, channel radius r_{cp}, and reduced width θ^2. In Eq. (4), the resonant term typically used in such calculations is augmented by taking into account the "potential scattering" contribution $A_{jl}^{(p)}$. This allows additional tests of reliability of the obtained results. The potential scattering term can be approximated reasonably well by the scattering off a solid sphere with radius r_{sp}:

$$A_{jl}^{(p)}(E) = -\frac{2F_l(kr_{sp})}{\sqrt{\Gamma(E)}} \frac{G_l(kr_{sp}) - iF_l(kr_{sp})}{F_l^2(kr_{sp}) + G_l^2(kr_{sp})} . \tag{6}$$

From Eq. (3) the amplitude is factorized into a momentum-dependent term and a radial integral

$$A_\gamma^{JM_J}(\Omega_x) = \frac{V_\gamma^J}{4}\,[j_1 \otimes j_2]_{JM_J}\, A_{j_1 l_1}(E_1)\, A_{j_2 l_2}(E_2),$$
$$V_\gamma^J = \int_0^R dr_1' \int_0^R dr_2'\, \hat{\psi}_{j_1 l_1}(E_{r1}, r_1')\, \hat{\psi}_{j_2 l_2}(E_{r2}, r_2') \times \Delta V(r_1', r_2')\, \varphi_{J\gamma}(r_1', r_2'). \quad (7)$$

Because the spin degrees of freedom cannot be observed even in the most sophisticated modern radioactive-ion-beam experiments, the summation over the final state spin quantum number is performed. For systems with zero core spin there are two terms to be treated. The first type is with $S = 0$ where $J = L$, and the second is with $S = 1$ where $L = \{J-1, J, J+1\}$. After averaging over M_J, it is obtained that

$$\frac{d\Gamma(E_{3r})}{d\Omega_x} = \sum_{LS} \frac{E_{3r}}{2\pi(2L+1)} \sum_{M_L} \left| \sum\nolimits_\gamma A_{S\gamma}^{LM_L}(\Omega_x) \right|^2, \quad (8)$$

$$A_{S\gamma}^{LM_L}(\Omega_x) = C_\gamma^{JLS}\, V_\gamma^J\, [l_1 \otimes l_2]_{LM_L}\, A_{j_1 l_1}(E_1) A_{j_2 l_2}(E_2), \quad (9)$$

$$[l_1 \otimes l_2]_{LM_L} = \sum\nolimits_{m_1 m_2} C_{l_1 m_1 l_2 m_2}^{LM_L} Y_{l_1 m_1}(\hat{r}_1) Y_{l_1 m_1}(\hat{r}_1).$$

The coefficient C_γ^{JLS} provides the jj to LS re-coupling for two protons in the orbitals j_1 and j_2:

$$C_{j_1 l_1 j_2 l_2}^{JLS} = \hat{L}\hat{S}\hat{j}_1\hat{j}_2 \begin{Bmatrix} l_1 & l_2 & L \\ 1/2 & 1/2 & S \\ j_1 & j_2 & J \end{Bmatrix}.$$

The potential matrix elements V_γ^J can be reasonably approximated [7,10] as

$$V_\gamma^J = c_\gamma^J \sqrt{[E_{r1} + E_{r2} - E_T]^2 + [\Gamma_1(E_{r1}) + \Gamma_2(E_{r2})]^2/4},$$

where c_γ^J are phenomenological complex coefficients, all normalized to unity, as $\sum_\gamma |c_\gamma^J|^2 \equiv 1$. The expression in Eq. (9) uses intermediate states in the subsystems with appropriate sets of quantum numbers and correctly couples them to the total spin of the system. However, there are important drawbacks in the approximation which do not allow the reproduction of realistic momentum distributions of fragments in $2p$ decays.

Therefore, a phenomenological improvement of Eq. (9) is proposed by replacing the amplitude with a more realistic one. The latter uses terms composed in different Jacob systems instead of those in the "V" system. For the case without potential scattering contribution in Eq. (4), it reads

$$A_{S\gamma}^{LM_L}(\Omega_x) \to \hat{\mathcal{O}}_S \left(\left[l_x^{Y_1} \otimes l_y^{Y_1} \right]_{LM_L} A_{j_x^{Y_1} l_x^{Y_1}}(E_x^{Y_1}) \sqrt{\Gamma_2(E_y^{Y_1})} + \left[l_x^{Y_2} \otimes l_y^{Y_2} \right]_{LM_L} \sqrt{\Gamma_1(E_y^{Y_2})}\, A_{j_x^{Y_2} l_x^{Y_2}}(E_x^{Y_2}) \right) \times \frac{C_\gamma^{JLS}\, V_\gamma^J\, A_S^{(pp)}(E_x^T)}{E_T - E_{r1} - E_{r2} + i\,[\Gamma_1(E_x^{Y_1}) + \Gamma_2(E_x^{Y_2}]/2}. \quad (10)$$

The permutation operator $\mathcal{O}_S$ provides the correct symmetry of the WFs with respect to proton permutations. As the isospin WFs of two protons are symmetric, it should be used as

$$\hat{\mathcal{O}}_0 \equiv \mathcal{S}, \qquad \hat{\mathcal{O}}_1 \equiv \mathcal{A}.$$

The amplitude $A_S^{(pp)}$ introduces corrections for the p–p final state interactions both for the $S = 0$ and $S = 1$ states of the two protons. The following expression is used:

$$A_S^{(pp)}(E_x^T) = \frac{N}{v_x^T} \sqrt{\frac{2}{\pi}} \int_0^\infty dr\, \psi_{l=S}^{(pp)}(k_x^T r)\, \phi(r), \quad (11)$$

where k_x^T and v_x^T are momentum and velocity associated with the p–p energy E_x^T. The meaning of such an approximation is to treat the protons as being emitted from a broad spatial region defined by the function $\phi(r)$. The source function $\phi(r)$ with a Gaussian type formfactor is used

$$\phi(r) = \frac{1}{a_{pp}^{3/2}} \sqrt{\frac{54}{\pi}}\, r \exp\left(-\frac{3r^2}{4a_{pp}^2} \right). \quad (12)$$

The radius parameter a_{pp} in the above expression is equal to the root mean square radius of the function $\phi(r)$. The simple singlet p–p potential $V(r) = -V_0 \exp[-(r/r_0)^2]$ with $V_0 = -31$ MeV and $r_0 = 1.8$ fm is used to define the s-wave proton scattering WF $\psi_{l=0}^{(pp)}$. The zero nuclear interaction is assumed for the p-wave p–p motion $\psi_{l=1}^{(pp)}$. The normalization coefficient N is chosen such that for a fixed three-body decay energy E_T

$$\int_0^1 d\varepsilon \sqrt{\varepsilon(1-\varepsilon)}\, |A_S^{(pp)}(\varepsilon E_T)|^2 = \pi/8. \quad (13)$$

In the calculations, $a_{pp} = 4$ fm is used, for which $|A_S^{(pp)}(E)|^2$ closely resembles the free p–p scattering cross section profile; a difference appears at small E values, where $A_S^{(pp)}(E)$ has the correct asymptotic behavior.

The IDDM unifies the advantages of both the NPP and EFC models and also goes beyond, thus providing a reliable tool for quantitative estimates and a phenomenological description of $2p$ decays.

(i) It can be shown, that Eq. (10) returns exactly Eq. (9) in the approximation $A_c \gg 1$, $Z_c \gg 1$, $A_S^{(pp)} \to 1$. Thus, the improved expression shows the proper transition to the previously used models.
(ii) The spins of the resonances in the subsystems and total angular momentum coupling schemes are correctly accounted in the proposed expressions as well as the proper symmetries of two-proton amplitudes.
(iii) In the present model two resonances can be treated simultaneously in two core + p subsystems without the infinite-core-mass assumption.
(iv) The proton–proton final state interaction is treated in a phenomenologically sufficient way.

4. Application to ^{16}Ne decays

In the following, the IDDM is applied to the examples of the ^{16}Ne 0^+ g.s. and the 2^+ first excited state, both decaying to $^{14}\mathrm{O} + p + p$, and its properties and performance is illustrated. In Refs. [10,20], the ^{16}Ne decay data have been compared with sophisticated full-scale three-body calculations. The comparison yields quantitative agreement, therefore the results of the detailed three-body calculations are used as a reference for the results obtained in the present work. This allows a direct and general comparison and avoids the use of Monte-Carlo (MC) simulations. The latter are needed for a realistic comparison of the semi-analytical model results with the data, which comprise the bias of the particular detector setup. In Fig. 4 the energy and angular distributions are presented, and widths are given in Table 1. It is assumed that a single configuration is involved in the decay: $[s_{1/2}^2]_0$ for the 0^+ state and $[s_{1/2}d_{5/2}]_2$ for the 2^+ state. The corresponding $\{E_r, \Gamma_r\}$

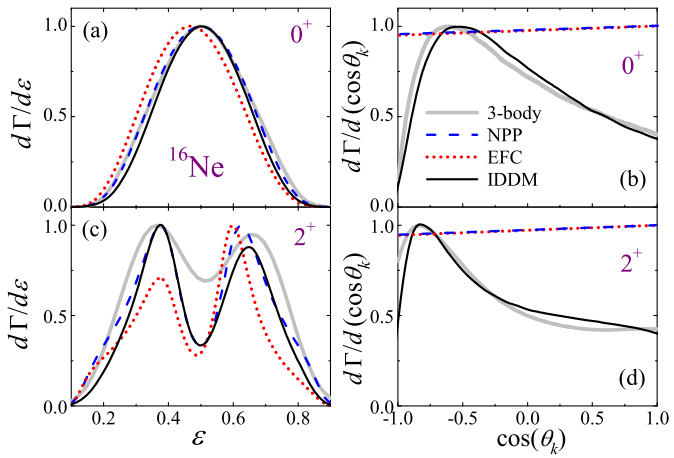

Fig. 4. (Color online.) Energy and angular distributions in the Jacobi "Y" system calculated by the 3-body, NPP, EFC, and IDDM models for the decay of the ^{16}Ne 0^+ g.s. (a,b) and the 2^+ first excited state (c,d).

Table 1
Widths (in keV) of ^{16}Ne states calculated with the NPP, EFC, IDDM and 3-body models. The decay energy of the 0^+ state is $E_T = 1.466$ MeV, and that of the 2^+ state is $E_T = 3.16$ MeV.

Γ (keV)	NPP	EFC	IDDM	3-body	Exp.
0^+	4.6	2.4	4.1	3.1	< 80 [20]
2^+	14	11	12	56	175 ± 75 [10]

sets in ^{15}F are $\{1.405, 0.7\}$ for $s_{1/2}$ and $\{2.8, 0.37\}$ for $d_{5/2}$. The contributions of the $[s^2_{1/2}]_0$ and $[s_{1/2}d_{5/2}]_2$ configurations in the structure of ^{16}Ne are taken as 67% [21] and 16% [10].

The different models yield the following results given in Table 1. The NPP model tends to overestimate the decay width [14]. The results of the IDDM lie in between the NPP and EFC width values. The NPP and EFC models also have different deficiencies in describing the momentum distributions of the $2p$ decay. The IDDM model reproduces all features of the momentum distributions qualitatively correct, see Fig. 4. Also a quantitative agreement with the full-scale three-body calculations is largely obtained. For example, one should note the correct positions and intensity-ratio of the two peaks in Fig. 4 (c). For the 2^+ state, however, a complete agreement with full-scale three-body calculations is not expected, as several quantum configurations are needed for description of the data [10].

As an intermediate result, the example of ^{16}Ne decays shows that the proposed IDDM combines the advantages of the NPP and EFC models, and it provides results which are close to the sophisticated three-body calculations. This makes the proposed approach a reasonable substitute for complicated three-body calculations, at least for exploratory and systematics studies.

5. Transition patterns in the *s–d* shell nuclei

In this Section, the IDDM will be applied more generally to several s–d shell nuclei and the decay dynamics is studied. The first case is ^{30}Ar decaying to $^{28}\mathrm{S} + p + p$ via the $[s^2_{1/2}]_0$ configuration, see Fig. 5. In the calculation, the $\{E_T, \varepsilon\}$ plane is scanned for a fixed proton resonance energy $E_r(^{29}\mathrm{Cl}) = 1.8$ MeV and several decay widths $\Gamma_r(^{29}\mathrm{Cl}) = 60, 170, 330, 500$ keV. In the considered "Y" Jacobi system $\varepsilon = E(\mathrm{core}\text{–}p)/E_T$ is the relative energy content of the core $+ p$ subsystem.

Transitions between different decay mechanisms become visible and the following evolution pattern can be recognized in Fig. 5 (a). At low E_T values, the true $2p$ decay mechanism prevails, which is characterized by a relatively narrow, bell-shaped distribution centered at $\varepsilon \sim 1/2$ (i.e., where the energies of both protons are equal). For $E_T > E_r$, two new peaks, associated with the sequential emission of protons, appear on the rising and falling edge of the central bell-shaped distribution. At an energy of $E_T \sim 1.2E_r \sim 2.2$ MeV, the sequential-emission peaks become higher than the central peak around $\varepsilon \sim 1/2$, and this value marks the transition point to the sequential decay mechanism (this was already sketched in Fig. 1 using the label "True $2p$"↔"Sequential $2p$" transition). Overall, the triangular structure reflects the evolution of the double-peak sequential decay pattern as a function of E_T. At the tip of the triangle, at $E_T = 2E_r$, the two peaks belonging to the sequential emission overlap; at still higher E_T they split up again.

Fig. 5 (b,c,d) shows the results for different, larger widths Γ_r, which is achieved by variation of the reduced width θ^2 parameter in Eq. (5). At first glance, similar patterns are obtained as for case (a). In detail, one can see that with increasing Γ_r the triangular sequential-decay pattern arises at higher energy E_T. However, it gradually smears out, and finally vanishes with increase of Γ_r. This qualitative difference reflects the transition to the democratic decay mechanism: the evolution observed in the decay patterns from (b) to (d) corresponds to the "Sequential $2p$"↔"Democratic $2p$" transition regime (which is also indicated in Fig. 1).

The panels (a) and (b) in Fig. 5 correspond to the θ^2 values of 0.5 and 2, respectively. The first value should correspond to the structure of a nucleus with strong configuration mixing. The second value is the upper limit of the admissible range for θ^2, which corresponds to a pure single-particle structure. The difference between the discussed E_T evolution patterns is quite significant. For instance, the transition "True $2p$"↔"Sequential $2p$" in the calculation (b) takes place at an E_T value, which is about 300 keV larger than that in the case (a). Unrealistically large θ^2 values of 4 and 6 are used in cases (c) and (d), respectively. They are considered for the study of the transition to the democratic $2p$-decay mechanism. From these and analogous evaluations it is found that the "True $2p$"↔"Democratic $2p$" transition takes place when the width Γ_r is described by the relation

$$\Gamma_r = \Gamma(E_r) \sim (0.2\text{–}0.3)E_r\,, \tag{14}$$

for this, see also Fig. 1.

It is obvious that the charge of ^{30}Ar is too large (hence the ^{29}Cl g.s. width is too small) to allow the democratic decay mechanism to materialize with the $E_r = 1.8$ MeV value used. The evolution of $2p$-decay mechanisms similar to the one shown in Fig. 5 (a)→(d) can be achieved by variation of a charge of the $2p$ precursor or/and energy E_r. Fig. 6 illustrates this issue by presenting three examples of the calculated transition patterns ranging from light to heavy s–d shell $2p$ emitters. In the calculated cases of ^{15}Ne, ^{26}S, and ^{34}Ca g.s. decays, it can be seen that the observed (^{15}Ne) as well as the evaluated (^{26}S) separation energies provide the g.s. location near the transition points. This means that it can be expected that the latter cases exhibit a strong sensitivity of the decay correlation patterns to the parameters of the involved nuclear states. In the following section, these findings will be utilized to study the core $+ p$ subsystem of a core $+ p + p$ nucleus.

6. Decay of the ^{15}Ne ground state

The first illustration, where the $2p$-decay transition dynamics is used to study the core $+ p$ subsystem, is provided by the ^{15}Ne g.s. decay. One can see in Fig. 6 (a), that the $2p$-decay energy of ^{15}Ne g.s., $E_T(\mathrm{exp}) = 2.52$ MeV [11], is located in the region where the width of the ε-distribution strongly varies with E_T. The shape of the ε-distribution *by itself* can be seen as a not very reliable, model-dependent indicator. However, the width of the ^{15}Ne g.s. is

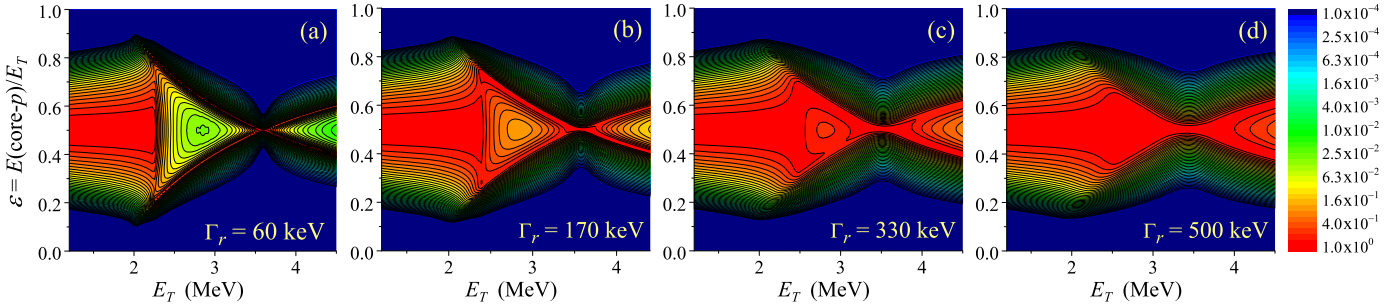

Fig. 5. (Color online.) Energy correlations as a function of the $2p$-decay energy E_T calculated by IDDM in the "Y" Jacobi system for ^{30}Ar. The ^{29}Cl $1/2^+$ g.s. energy is $E_r = 1.8$ MeV. The panels (a, b, c, d) correspond to the assumed $\Gamma_r(^{29}\text{Cl})$ values of 60, 170, 330, 500 keV, respectively. The distributions for each energy E_T are normalized to unity maximum value.

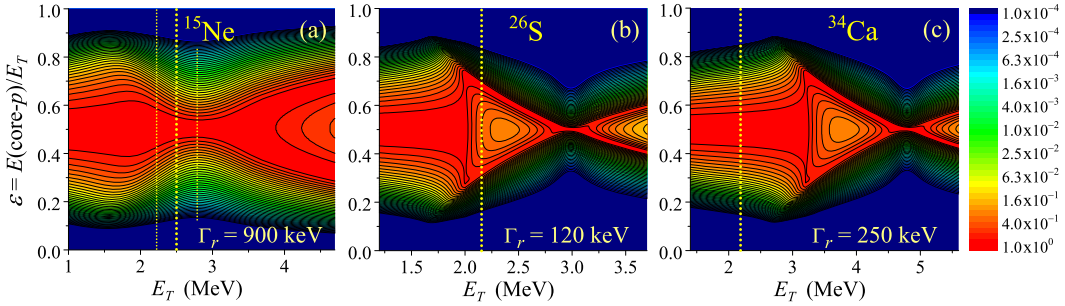

Fig. 6. (Color online.) Energy correlations as a function of the $2p$-decay energy E_T calculated by IDDM in the "Y" Jacobi system for ^{15}Ne, ^{26}S, and ^{34}Ca. The corresponding $\{E_r, \Gamma_r\}$ values are {1.56, 0.9} (both values taken from the experiment in Ref. [22]), {1.51, 0.12}, {2.41, 0.25} (E_r from [13], Γ_r calculated assuming an s-wave decay with $\theta^2 = 2$, which is the single-particle limit). The vertical dotted lines mark the E_T values from the experiment for ^{15}Ne [11] as well as from the systematics [13] for the cases ^{26}S and ^{34}Ca. The thin dotted lines for ^{15}Ne indicate the E_T region within experimental value of the g.s. width $\Gamma = 0.59$ MeV [11]. The distributions for each energy E_T are normalized to unity maximum value.

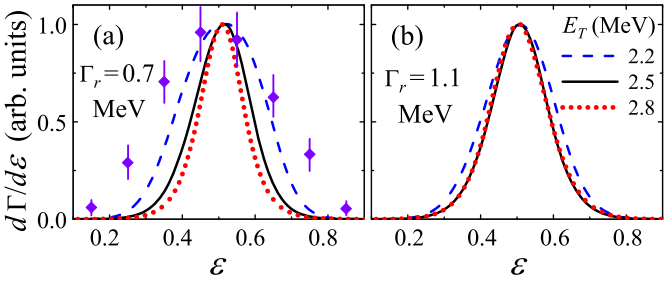

Fig. 7. (Color online.) Energy distributions of the $2p$ decay products of ^{15}Ne (dots, with statistical uncertainties, in the "Y" Jacobi system [11]) calculated at three E_T values (in MeV) of the ^{15}Ne g.s. The ^{14}F g.s. width is assumed to be either 0.7 MeV (a) or 1.1 MeV (b).

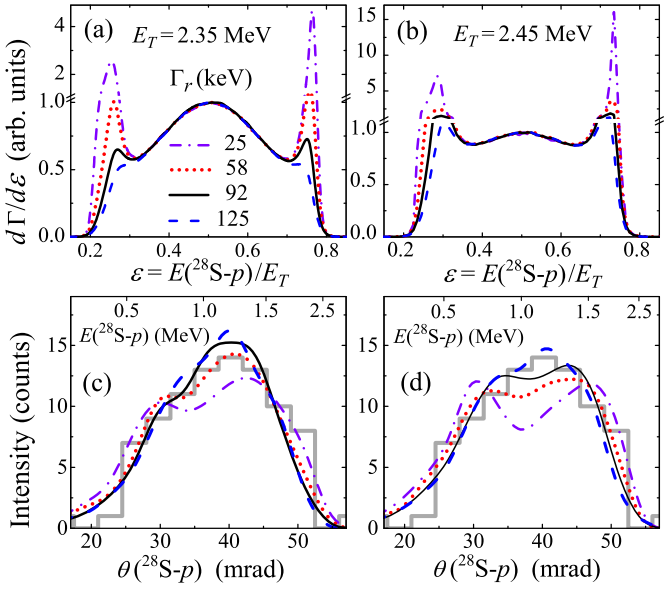

Fig. 8. (Color online.) Energy distributions of the $2p$-decay products of ^{30}Ar, calculated in the "Y" Jacobi system for the two E_T values shown in panels (a) and (b). The $E_r = 1.8$ MeV value is fixed, while the curves represent different Γ_r values. In panels (c) and (d), the experimental angular distribution between core and one of the protons measured for ^{30}Ar g.s. decay in Ref. [12] (histograms) is compared with those from the respective theoretical distributions shown in panels (a) and (b). The experimental bias is taken into account in the Monte-Carlo simulations.

quite broad, $\Gamma(\text{exp}) = 0.59$ MeV, and one may in addition investigate the *evolution* of the ε distribution as function of E_T depending on model parameters. In Fig. 7 the "Y" system ε-distributions are calculated for different decay energies of ^{15}Ne within the g.s. resonance peak (namely, $E_T(\text{exp})$ and $E_T(\text{exp}) \pm \Gamma(\text{exp})/2$), and for different widths of the ^{14}F g.s. within the experimental uncertainty for this value. Ref. [22] provides $E_r(\text{exp}) = 1.56(4)$ MeV and $\Gamma_r(\text{exp}) = 0.9(2)$ MeV for ^{14}F g.s., so the values $\Gamma_r = 0.7$ and $\Gamma_r = 1.1$ are used for calculations in Fig. 7.

As expected, the ε-distributions, calculated for the centroid (E_T) and for the limiting cases ($E_T \pm \Gamma/2$) of the ^{15}Ne g.s. resonance, differ from each other. In particular, the differences are quite pronounced with respect to the different values of the ^{14}F g.s. widths $\Gamma_r(^{14}\text{F})$, which, in turn, allows to extract some information on the widths Γ_r from the ^{15}Ne decay correlation data. The data for ^{15}Ne g.s. measured in Ref. [11] are shown in Fig. 7 (a). A direct quantitative comparison is not appropriate, since the measured distribution is broadened by the experimental resolution and the counts is not sufficient to study the E_T evolution in detail. However, we would like to mention that such an analysis is possible with better statistics and better experimental resolution, as can

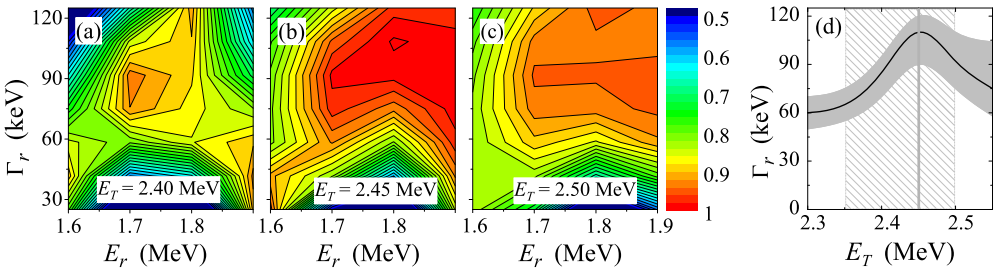

Fig. 9. (Color online.) Panels (a,b,c) show the likelihood of agreement between theoretical and experimental angular distributions (see Fig. 8) of $2p$-decays of the ^{30}Ar g.s. The probability is shown as function of the $\{E_r, \Gamma_r\}$ variables for fixed E_T values as indicated in the panels. Panel (d) shows the band of $\{\Gamma_r, \Delta\Gamma_r\}$ values correlated with E_T. The best-fit E_T value and its 1σ-uncertainty are indicated by the vertical line and the hatched area, respectively.

be seen in the similar example of the ^{16}Ne g.s. decay [20]. The precision of the latter experiment seems to be sufficient to distinguish the solid and dotted curves in Fig. 7 (a) or dashed and solid curves in Fig. 7 (b). So, the proposed analysis is in principle feasible.

7. Decay of the ^{30}Ar ground state

The observation and study of the new isotopes ^{30}Ar and ^{29}Cl were reported recently [12]. It was concluded that the $2p$ decay of the ^{30}Ar g.s. is located in the transition regime between true $2p$ and sequential $2p$ decays. The analysis was carried out in a simplified way with the decay energy as the only parameter. Here, the ^{30}Ar data are re-analyzed using IDDM calculations.

Several calculated correlations and the respective "experimental" distributions (simulated by taking into account the setup response function, along the lines described in [12]) are shown in Fig. 8 together with the experimental data. Despite strong effects of the experimental setup, the measured angular distributions of the $2p$-decay products appear to be informative. One can see from the figure, that the specific patterns connected with the formation of sequential-decay correlations of the ^{30}Ar g.s. produce sizable changes in the angular distributions $^{28}\mathrm{S} + p$.

In order to find the best match with experimental data, the parameters $\{E_T, E_r, \Gamma_r\}$ were systematically varied; a Kolmogorov test provides the probability for agreement between simulation results and experimental histograms, see Fig. 9. In the previous study Ref. [12], the assigned parameters were $E_T = 2.25^{+0.15}_{-0.10}$ MeV, $E_r = 1.8(1)$ MeV. On the basis of the present, more refined analysis, whose results are shown in Fig. 9, a more precise value $E_T = 2.45^{+0.05}_{-0.10}$ MeV is inferred (in agreement with our previous findings), and also the width of ^{29}Cl g.s. is derived as $\Gamma_r = 85(30)$ keV. A pleasant feature of this analysis is that uncertainties of the major parameters are correlated, which can be used for imposing further limits. For example, it is shown in Fig. 9 (d) that a smaller $\Delta\Gamma_r \sim 15$ keV can be established for a fixed E_T value.

It should be emphasized that the analysis performed is in the "proof of concept" stage, and should be validated by direct measurements.

8. Sensitivity of IDDM results

The reliability of the proposed width determination of a core $+ p$ g.s. nuclear system from the energy distributions obtained in the "Y" coordinate system depends on the robustness of the distributions with respect to the model parameters used. Such a sensitivity was systematically investigated, and it was found that the only significant dependence results from the general decay parameters $\{E_T, E_r, \Gamma_r\}$. For instance, the transition patterns strongly depend on the interference of two-body amplitudes at resonant and near-resonant energy. However, Fig. 10 shows that a modification of amplitudes outside the resonance peak does not lead to significant changes of the characteristic behavior.

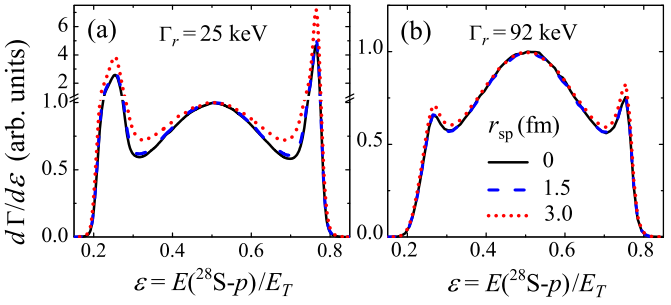

Fig. 10. (Color online.) Sensitivity of energy distributions in the "Y" system to modifications of amplitudes (4) by "potential scattering" contributions (6) with different r_{sp}. The example shows the case ^{30}Ar (see Fig. 8) with $E_T = 2.35$ MeV, $E_r = 1.8$ MeV and two different Γ_r values.

The other important assumption is that only one quantum configuration provides a dominating contribution to the decay width of the state. However, this is a natural situation for the transition dynamics, which is connected to the strong variation of the partial width just in one selected channel. This may be estimated in a forthcoming theoretical study.

9. Summary

Nearly half of the neutron-deficient s–d shell nuclei located 1–2 neutron numbers beyond the proton dripline decay by $2p$ emission. This decay mode exhibits three different characteristic: true $2p$, democratic and sequential decay mechanisms. Their occurrence depends mainly on the relationship of the three parameters E_T, E_r, and Γ_r. The changeover from one decay mechanism to another, which is reflected by altered momentum distributions of the decay products, occurs within rather narrow transition areas, i.e. within small changes of the relevant $2p$-decay parameters. The behavior of the momentum distributions of $2p$-decay products in the transition regions can be described by the semi-analytical improved direct decay formalism, IDDM. At variance to previously used approximations, the IDDM depicts all qualitative features of $2p$-decay distributions in the whole kinematical space; in particular it covers the mentioned $2p$-decay transition regions. Even with moderate computing effort, this model yields reliable quantitative estimates and phenomenological evidence, ideally suited for large-scale systematic surveys. Further development and refinements of such a model are of importance for future studies. In the transition regions, the momentum distributions of the decay products exhibit a strong sensitivity with respect to the variation of the three general $2p$-decay parameters. Therefore experimental data from the $2p$ correlations in transition regions can be used to extract resonance parameters in the core $+ p$ subsystem of the $2p$-decay

precursor. The practical feasibility of such an approach has been demonstrated here with the example of the ^{15}Ne g.s. $2p$-decay. By relying on the transition dynamics, improved constraints for the parameters E_T, E_r, and Γ_r for the ^{30}Ar and ^{29}Cl g.s. can be set in comparison with the values derived in Ref. [12]. Overall, this will contribute to a better understanding of structure and decay dynamics of nuclei and resonances at and beyond the driplines.

Acknowledgements

T.A.G. was partly supported by the Flerov laboratory JINR and by the Helmholtz International Center for FAIR (HIC for FAIR) within the framework of the LOEWE program launched by the State of Hessen. X.X. acknowledges the support from the same HIC for FAIR grant. L.V.G. was partly supported by the Russian Foundation for Basic Research grant No. 14-02-00090. The authors thank J.S. Winfield for carefully proofreading the manuscript.

References

[1] V.I. Goldansky, Nucl. Phys. 19 (1960) 482–495.
[2] M. Pfützner, E. Badura, C. Bingham, B. Blank, M. Chartier, H. Geissel, J. Giovinazzo, L.V. Grigorenko, R. Grzywacz, M. Hellström, Z. Janas, J. Kurcewicz, A.S. Lalleman, C. Mazzocchi, I. Mukha, G. Münzenberg, C. Plettner, E. Roeckl, K.P. Rykaczewski, K. Schmidt, R.S. Simon, M. Stanoiu, J.C. Thomas, Eur. Phys. J. A 14 (2002) 279.
[3] J. Giovinazzo, B. Blank, M. Chartier, S. Czajkowski, A.L. Fleury, M.J. Jimenez, M.S. Pravikoff, J.C. Thomas, F. de Oliveira Santos, M. Lewitowicz, V. Maslov, M. Stanoiu, R. Grzywacz, M. Pfützner, C. Borcea, B.A. Brown, Phys. Rev. Lett. 89 (10) (2002) 102501.
[4] M. Pfützner, M. Karny, L.V. Grigorenko, K. Riisager, Rev. Mod. Phys. 84 (2012) 567–619.
[5] O.V. Bochkarev, et al., Nucl. Phys. A 505 (1989) 215.
[6] L.V. Grigorenko, M.V. Zhukov, Phys. Rev. C 68 (2003) 054005.
[7] L.V. Grigorenko, M.V. Zhukov, Phys. Rev. C 76 (2007) 014008.
[8] I. Mukha, L. Grigorenko, L. Acosta, M.A.G. Alvarez, E. Casarejos, A. Chatillon, D. Cortina-Gil, J.M. Espino, A. Fomichev, J.E. García-Ramos, H. Geissel, J. Gómez-Camacho, J. Hofmann, O. Kiselev, A. Korsheninnikov, N. Kurz, Y.A. Litvinov, I. Martel, C. Nociforo, W. Ott, M. Pfützner, C. Rodríguez-Tajes, E. Roeckl, C. Scheidenberger, M. Stanoiu, K. Sümmerer, H. Weick, P.J. Woods, Phys. Rev. C 85 (2012) 044325.
[9] I.A. Egorova, R.J. Charity, L.V. Grigorenko, Z. Chajecki, D. Coupland, J.M. Elson, T.K. Ghosh, M.E. Howard, H. Iwasaki, M. Kilburn, J. Lee, W.G. Lynch, J. Manfredi, S.T. Marley, A. Sanetullaev, R. Shane, D.V. Shetty, L.G. Sobotka, M.B. Tsang, J. Winkelbauer, A.H. Wuosmaa, M. Youngs, M.V. Zhukov, Phys. Rev. Lett. 109 (2012) 202502.
[10] K.W. Brown, R.J. Charity, L.G. Sobotka, L.V. Grigorenko, T.A. Golubkova, S. Bedoor, W.W. Buhro, Z. Chajecki, J.M. Elson, W.G. Lynch, J. Manfredi, D.G. McNeel, W. Reviol, R. Shane, R.H. Showalter, M.B. Tsang, J.R. Winkelbauer, A.H. Wuosmaa, Phys. Rev. C 92 (2015) 034329.
[11] F. Wamers, J. Marganiec, F. Aksouh, Y. Aksyutina, H. Álvarez-Pol, T. Aumann, S. Beceiro-Novo, K. Boretzky, M.J.G. Borge, M. Chartier, A. Chatillon, L.V. Chulkov, D. Cortina-Gil, H. Emling, O. Ershova, L.M. Fraile, H.O.U. Fynbo, D. Galaviz, H. Geissel, M. Heil, D.H.H. Hoffmann, H.T. Johansson, B. Jonson, C. Karagiannis, O.A. Kiselev, J.V. Kratz, R. Kulessa, N. Kurz, C. Langer, M. Lantz, T. Le Bleis, R. Lemmon, Y.A. Litvinov, K. Mahata, C. Müntz, T. Nilsson, C. Nociforo, G. Nyman, W. Ott, V. Panin, S. Paschalis, A. Perea, R. Plag, R. Reifarth, A. Richter, C. Rodriguez-Tajes, D. Rossi, K. Riisager, D. Savran, G. Schrieder, H. Simon, J. Stroth, K. Sümmerer, O. Tengblad, H. Weick, C. Wimmer, M.V. Zhukov, Phys. Rev. Lett. 112 (2014) 132502.
[12] I. Mukha, L. Grigorenko, X. Xu, L. Acosta, E. Casarejos, W. Dominik, J. Duénas-Díaz, V. Dunin, J. Espino, A. Estradé, F. Farińon, A. Fomichev, H. Geissel, T. Golubkova, A. Gorshkov, Z. Janas, G. Kamiński, O. Kiselev, R. Knöbel, S. Krupko, M. Kuich, A. Lis, Y. Litvinov, G. Marquinez-Durán, I. Martel, C. Mazzocchi, C. Nociforo, A. Ordúz, M. Pfützner, S. Pietri, M. Pomorski, A. Prochazka, S. Rymzhanova, A. Sánchez-Benítez, C. Scheidenberger, P. Sharov, H. Simon, B. Sitar, R. Slepnev, M. Stanoiu, P. Strmen, I. Szarka, M. Takechi, Y. Tanaka, H. Weick, M. Winkler, J. Winfield, M. Zhukov, Phys. Rev. Lett. 115 (2015) 202501.
[13] J. Tian, N. Wang, C. Li, J. Li, Phys. Rev. C 87 (2013) 014313.
[14] L.V. Grigorenko, M.V. Zhukov, Phys. Rev. C 76 (2007) 014009.
[15] V.M. Galitsky, V.F. Cheltsov, Nucl. Phys. 56 (1964) 86–96.
[16] W. Fowler, G. Caughlan, B. Zimmerman, Annu. Rev. Astron. Astrophys. 5 (1967) 525.
[17] B.A. Brown, F.C. Barker, Phys. Rev. C 67 (2003) 041304.
[18] F.C. Barker, Phys. Rev. C 68 (2003) 054602.
[19] L.V. Grigorenko, Phys. Part. Nucl. 40 (2009) 674–714.
[20] K.W. Brown, R.J. Charity, L.G. Sobotka, Z. Chajecki, L.V. Grigorenko, I.A. Egorova, Y.L. Parfenova, M.V. Zhukov, S. Bedoor, W.W. Buhro, J.M. Elson, W.G. Lynch, J. Manfredi, D.G. McNeel, W. Reviol, R. Shane, R.H. Showalter, M.B. Tsang, J.R. Winkelbauer, A.H. Wuosmaa, Phys. Rev. Lett. 113 (2014) 232501.
[21] L.V. Grigorenko, T.A. Golubkova, M.V. Zhukov, Phys. Rev. C 91 (2015) 024325.
[22] V. Goldberg, B. Roeder, G. Rogachev, G. Chubarian, E. Johnson, C. Fu, A. Alharbi, M. Avila, A. Banu, M. McCleskey, J. Mitchell, E. Simmons, G. Tabacaru, L. Trache, R. Tribble, Phys. Lett. B 692 (5) (2010) 307–311.